Pulled array continuous electrical sounding with an additional inductive source: an experimental design study

Niels B. Christensen* and Kurt Sørensen

Department of Earth Sciences, Aarhus University, Finlandsgade 8, DK-8200 Aarhus N, Denmark

ABSTRACT

Electrical and electromagnetic profiling methods are used extensively in environmental geophysical investigations for many different purposes. The pulled array continuous electrical sounding (PACES) method, where a tail of electrodes is towed behind a small vehicle while continuously and simultaneously measuring several electrode configurations, has been used extensively for mapping the vulnerability of aquifers in Denmark. Measurements are taken every 1 m, and 10–15 km of profile can be achieved in one day.

This paper presents a theoretical study of the resolution capabilities of PACES measurements as they are now performed, and an experimental design study for including an inductive source in the measuring equipment. The joint interpretation of the galvanic data set of ordinary PACES measurements with inductive data from a horizontal magnetic dipole source will enhance the resolution capabilities of the data set significantly. The study is carried out as an analysis of the uncertainty of the model parameters of one-dimensional three-layer models using the estimation error variances of the inversion problem.

The results indicate that the addition of only two frequency data from a magnetic dipole source will substantially improve the resolution of the subsurface resistivity structure. The improvement is model dependent, but reduction in the relative error of model parameters by an order of magnitude is observed.

INTRODUCTION

Geological mapping of the near-surface of the earth is of vital importance in many contexts in environmental geophysics. Prospecting for raw materials, hydrogeological investigations of the vulnerability of aquifers, and the mapping of dump sites prior to remediation measures all benefit from high-resolution electrical and electromagnetic measurements. The results of interpretation of these data often yield the information necessary for subsequent decisions. The usefulness of such investigations is determined by the reliability of the data, the density of the measurements and the quality of the interpretation (Christensen and Sørensen 1998).

Geoelectrical profiling with steel rod electrodes, electromagnetic profiling with ground conductivity meters and Slingram-type equipment with multiple frequencies are the traditional methods for obtaining such data. Often, however, these methods turn out to be prohibitively expensive, when a dense grid of profile lines with several investigation depths is required.

The pulled array continuous electrical profiling (PACEP) and the pulled array continuous electrical sounding (PACES) methods (Sørensen 1995, 1996) are novel methods designed to fulfil the needs of modern near-surface investigations. A tail of electrodes with multiple configurations is towed behind a small vehicle and, while moving, 10 km of profile per day of geoelectrical data are measured at 1 m intervals along the profile line.

It is well known that a joint interpretation of galvanic

---

*E-mail: nbc@geo.au.dk

(conductive) and inductive data will yield a better resolution of the subsurface resistivity structure than any of the data sets separately (Jupp and Vozoff 1975). This leads naturally to the idea of including inductive measurements in the PACES method. A configuration has been chosen, where the electric field parallel to the tail due to a horizontal magnetic dipole perpendicular to the tail is measured. As will be shown, the addition of a few inductive measurements significantly enhances the resolution capabilities of the total data set. The improvements obtained by using one, two, three and four additional frequency data have been analysed by comparing the standard deviation of the model parameters and model parameter combinations of three-layer models based on the galvanic data alone with that of a combination of the galvanic and inductive data. The analyses based on the estimation error variances of the linearized inversion problem lead to an experimental design and have been carried out using the SELMA program (Christensen and Auken 1992).

Figure 1 Sketch of the PACES method with an inductive source and the electrode configurations of the eight-channel PACES system.

THE PACES METHOD

The PACES method is a development of its predecessor, the PACEP method, which included three electrode distances (Sørensen 1996).

The PACEP method has been used extensively to map the presence of near-surface clay layers and thus the vulnerability of underlying aquifers. The results of the measurements are presented as contoured resistivity maps, one for each electrode distance. Recently 2D interpretations along the profile lines based on a deconvolution algorithm using the Born approximation (Møller *et al.* 1996, 2001) have been used to produce contoured maps of mean resistivities in three depth intervals (Møller and Sørensen 1998), which give a considerable improvement on the estimates of resistivities in deeper parts of the earth.

Besides mapping near-surface capping clays, the maps produced from PACEP measurements have been used in connection with road construction and the mapping of raw materials such as sand, gravel and clays.

The PACES system comprises eight electrode configurations mounted on a 100 m long tail in Wenner or Wenner-like symmetric configurations plus pole–pole-like and pole–dipole-like configurations (see Fig. 1) and it essentially produces a continuous vertical electrical sounding. The two current electrodes have fixed positions, separated by 30 m, and the potential electrode configurations are distributed to produce electrode distances from a pole–pole-like

configuration with a 2 m spacing and a true Wenner configuration with a 30 m spacing.

The design of the PACES system was chosen subject to a number of constraints. The electrodes were placed at whole metre points to facilitate numerical multidimensional modelling. It is difficult to handle a tail much longer than 100 m in the field, which limits the maximum electrode separation to a 30 m Wenner configuration. To ensure adequate flexibility of the tail, the smallest electrode separation was chosen to be 2 m. Between these extremes, six electrode configurations were chosen in such a way that the distribution of sensitivity is homogeneous over the depth penetration range. Edwards (1977) defined the median depth of investigation as the depth where the integrated half-space Fréchet kernel (Oldenburg 1978) reaches half its maximum value. With this definition the configurations used in the PACES system have investigation depths between 1.53 m and 15.6 m, corresponding to a density of seven data per decade. The investigation depth range corresponds to a Schlumberger sounding with $L/2$-distances between 4 m and 40 m. Normally, a Schlumberger DC sounding is made with more than seven points per decade and the resolution capability of the PACES system must therefore be expected to be slightly inferior to that of a Schlumberger sounding with electrodes in the equivalent $L/2$-range. If the Schlumberger sounding is performed with a minimum $L/2$-distance smaller than 4 m, which is a common case, the Schlumberger sounding will naturally have a better resolution of the near-surface layers than the PACES data.

The primary source of error in the PACES galvanic data is the electrochemical potentials on the potential electrodes which do not vanish, due to the constant movement of the electrodes. Through band-pass filtering and predictive filtering of the measured potentials, the effective noise is reduced to approximately 2%. Besides the measurement error there are misalignment errors close to points where the profile direction changes. These parts of the profile are normally eradicated in the post-processing stage before interpretation. The misalignment errors due to stretching of the tail are very small thanks to the Kevlar® rope running through the tail. For the tensions arising in the field the stretching is less than 0.5%.

An area of 3000 km^2 corresponding to 9000 line kilometres has so far been covered using the PACEP and the PACES systems.

THE INDUCTIVE SOURCE

To this measuring system we propose adding a horizontal magnetic dipole source with its axis perpendicular to the tail and measuring the electric field in the direction of the tail. This configuration allows measurement of the secondary field with electrodes already mounted on the tail. Neither a vertical magnetic dipole nor a horizontal magnetic dipole with its axis parallel to the tail will produce an electric field in the direction of the tail. The dipole is mounted at the front end of the tail. The primary source field, i.e. the full-space field, has no electric field component in the direction measured and there is thus no need for compensation of the primary field, which is an important source of error in electromagnetic frequency-domain methods. However if, due to topography, the source dipole is elevated relative to the receiving electrodes, there will be a primary electric-field component in the direction measured. Terrain slopes in Denmark are typically smaller than 2%. The effect is proportional to the sine of the angle and is thus of first order. It is one of many effects arising when the earth is not one-dimensional (1D), but a thorough discussion of two-dimensional (2D) effects is beyond the scope of this paper.

With an additional horizontal magnetic dipole source, the errors due to misalignment of the magnetic dipole source must be taken into account. Rotational displacement about a horizontal axis perpendicular to the tail does, of course, not change the dipole source. Rotational displacement about a vertical axis will reduce the effective magnetic moment perpendicular to the tail and give a magnetic dipole moment in the direction of the tail. However, the magnetic moment in

the direction of the tail does not produce an electric field in the direction of the tail. Rotational displacement around a horizontal axis parallel to the tail will, besides reducing the effective moment perpendicular to the tail, introduce a vertical magnetic dipole moment which does also not produce an electric field in the direction of the tail. These considerations show that the only effect of misalignment of the horizontal magnetic dipole source on a 1D earth is the reduction of the effective moment. The effective moment is proportional to the cosine of the displacement angle, so the error is of second order.

The major source of error in the inductive data is probably caused by the coupling to man-made structures.

The electric field due to a horizontal magnetic dipole in the quasi-static approximation is calculated using the formula given by Ward and Hohmann (1987),

$$E_y = \frac{\partial F}{\partial x}, \tag{1}$$

where the Schelkunoff potential F is given by

$$F = -\frac{\hat{z}_0 m}{4\pi} \frac{\partial}{\partial x} \int_0^\infty \{\exp[-u_0(z+h)] + r_{TM} \exp[u_0(z-h)]\}$$

$$\times \frac{1}{\lambda} J_0(\lambda r) \, d\lambda, \tag{2}$$

where $\hat{z}_0 = i\omega\mu_0$, $h = 0$ is the height above ground of the magnetic dipole source, r_{TM} is the recursively obtained reflection coefficient at the surface and J_0 is the zero-order Bessel function of the first kind. The numerical calculations were performed using the SELMA program (Christensen and Auken 1992).

Figure 2 shows the amplitude of the electric field in a homogeneous half-space due to a horizontal magnetic dipole source with unit dipole moment as a function of the transmitter/receiver (Tx/Rx) distance for the two frequencies, 2 kHz and 20 kHz. Basically, the signal strength is proportional to the frequency. The transition between the near field with a decay proportional to distance squared and the far field with a decay proportional to the distance cubed is seen in the plots. The transition occurs approximately at a distance equal to the skin depth, which is 112 m for the frequency 2 kHz and 35 m for 20 kHz.

The electric field from the horizontal magnetic dipole source can be measured with electrodes already mounted on the tail, but equipped with separate phase-lock amplifiers. The signal from these is transmitted through the cable system as a low-voltage DC current, thus minimizing the capacitive coupling to the galvanic system. The magnetic dipole source is placed close to the cabling, but the resulting induction in
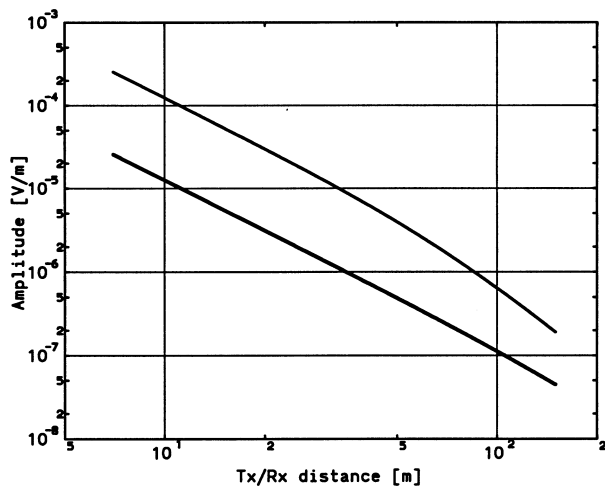
Figure 2 The amplitude of the in-line electric field from a horizontal magnetic dipole perpendicular to the electrode tail with unit dipole moment. The field is on a 100 Ωm half-space for the frequencies 2 kHz (lower curve) and 20 kHz (upper curve).

the cable can be suppressed by filtering since the frequency contents of the galvanic and the inductive signals are very different.

JOINT INVERSION OF GALVANIC AND INDUCTIVE DATA

Due to noise, there is a degree of uncertainty in the information provided by all geophysical data. This means that the physical interpretation of geophysical data always contains equivalence, i.e. there exists a set of models which all satisfy the data within the uncertainty of the measurements.

For 1D interpretation of electrical and electromagnetic data the more prominent equivalences have been given specific names. For galvanic data, high-resistivity equivalence, low-resistivity equivalence and layer suppression are the most important. For inductive data, there is low-resistivity equivalence, the inability to distinguish high resistivities, and layer suppression.

The high-resistivity equivalence encountered in the interpretation of galvanic data means that the resistivity and thickness of a high-resistivity layer embedded between layers of lower resistivities are undetermined unless the thickness of the high-resistivity layer is sufficiently large – as a rule of thumb, more than twice the thickness of the overburden. This is because models with the same product of resistivity and thickness, i.e. the vertical resistance, have rather similar responses. The vertical resistance of the layer is sometimes determined although the individual parameters are not.

Correspondingly, low-resistivity equivalence means that the resistivity and thickness of a low-resistivity layer embedded between layers of higher resistivities are undetermined unless the thickness of the low-resistivity layer is sufficiently large – as a rule of thumb, greater than the thickness of the overburden. This is because models with the same quotient of thickness and resistivity, i.e. the horizontal conductance, have rather similar responses. The horizontal conductance of the layer is sometimes determined although the individual parameters are not.

A layer may be too thin to be detected individually in an interpretation of electric and electromagnetic data, and the data set may be interpreted without the presence of the layer. This is the phenomenon of layer suppression. The critical thickness depends on the parameters of the whole model.

In contrast to galvanic data, which are sensitive to relative changes in resistivity/conductivity, inductive data are more adequately described as being sensitive to the absolute value of the conductivity. This causes high resistivities (low absolute conductivities) to be undetermined by inductive data. Often resistivities higher than 80–100 Ωm will not be resolved in detail. The detection of good conductors, however, is usually no problem for inductive data sets, and the depth to a good conductor is usually well determined.

Numerous studies have shown that the joint interpretation of galvanic and inductive data, where a single model is sought which satisfies both data sets, will generally enhance the resolution of the subsurface resistivity structure (e.g. Jupp and Vozoff 1975; Raiche *et al.* 1985; Sandberg 1993). Specifically, some of the equivalences encountered in the interpretation of galvanic data sets may be resolved or drastically reduced by including a few inductive data.

In the case of a layer showing high-resistivity equivalence, the inclusion of inductive data will most often determine the depth to the good conductor underlying the high-resistivity layer, and if the top boundary is resolved, the thickness is thereby determined. If the vertical resistance is determined, then the resistivity will also be determined, and the equivalence is resolved. Even in the case of low-resistivity equivalence exhibited by both galvanic and inductive data, the joint interpretation will reduce the equivalence (Fitterman, Meekes and Ritsema 1988). The problems with layer suppression will generally be reduced, as a joint interpretation will resolve thinner layers than will either data set alone. Also the weakness of the inductive data in resolving high resistivities is compensated for by the relative nature of galvanic data, and this equivalence is often removed by joint interpretations.

$\rho_1 = 100\,\Omega\mathrm{m}$	$d_1 = 5\,\mathrm{m}$
$\rho_2 = 10\text{-}1000\,\Omega\mathrm{m}$	$d_2 = 0.5\text{-}50\,\mathrm{m}$
$\rho_3 = 10\,/\,100\,/\,1000\,\Omega\mathrm{m}$	

Figure 3 The three-layer model used in the analyses.

Thus the inclusion of inductive data in the PACES data set must be expected to reduce problems with layer suppression, reduce the low-resistivity equivalence and drastically reduce the high-resistivity equivalence otherwise encountered with this method.

EXPERIMENTAL DESIGN – THE ANALYSES

Experience with joint interpretations suggests that a small number of additional inductive data will suffice to supplement the galvanic data set. Thus, an experimental design requires us to choose the *Tx/Rx* separation, the number of frequencies and the frequencies themselves. To this end, a series of analyses of 1D interpretations of a set of three-layer models have been made with *Tx/Rx* spacings equal to 45 m and 85 m and with one, two, three and four frequencies. The analyses have included all model parameters and model parameter combinations, i.e. the resistivities of the first, second and third layers, the thicknesses of the first and second layers and the depth to the third layer, the vertical resistance (resistivity times thickness) of the first and second layers and their sum, and correspondingly for the horizontal conductance (conductivity times thickness). For brevity, only a limited number of these analyses can be presented. For all analyses it was assumed that there is 2% noise on the DC resistivity data and the amplitude of the frequency data. The 2% level was chosen based on field experience with the PACES system.

Due to the, in principle, infinite number of data combinations, we have limited ourselves to a set of realizable possibilities. The data type was chosen to be the amplitude of the potential difference, thus discarding the phase. There may be problems associated with the measurement of the phase due to coupling phenomena of the cabling in the tail, and by assuming only amplitude data we are sure of avoiding these. However, one analysis of the influence of phase is given at the end of the paper. For the same reasons, the maximum frequency was chosen equal to 20 kHz, although higher frequencies could probably be made to work properly. All in all, these self-imposed restrictions give us conservative estimates.

The analyses are given by the relative uncertainty of the model parameters obtained as the square root of the diagonal elements of the covariance matrix $(\mathbf{A}^\mathrm{T}\mathbf{C}_\mathrm{e}^{-1}\mathbf{A})^{-1}$, where $\mathbf{A}$ is the Jacobian matrix containing the derivatives of the data with respect to the logarithm of the layer resistivities and layer thicknesses and $\mathbf{C}_\mathrm{e}$ is the data error covariance matrix. $\mathbf{C}_\mathrm{e}$ is chosen to be diagonal, corresponding to an assumption of uncorrelated noise on the data.

In Figs 4–10, the results of the analyses are presented as grey-scale images, referred to as 'templates'. The analyses are presented as contoured plots of the uncertainty of a specific model parameter or model parameter combination of three-layer models. RHO1, RHO2 and RHO3 indicate the resistivities of the first, second and third layers (ρ_1, ρ_2 and ρ_3), respectively. THICK1, THICK2 and DEPTH3 indicate the thicknesses of the first and second layers and the depth to the third layer (d_1, d_2 and $h_3 = d_1 + d_2$), respectively. RES1 and RES2 indicate the vertical resistances of the layers ($\rho_1 d_1$, $\rho_2 d_2$). CON1 and CON2 indicate the horizontal conductances of the layers (d_1/ρ_1, d_2/ρ_2).

The model (see Fig. 3) was chosen with $\rho_1 = 100\,\Omega\mathrm{m}$ and $d_1 = 5\,\mathrm{m}$. d_2 varies logarithmically along the horizontal axis of the template between $0.1d_1$ and $10d_1$ in 21 steps, corresponding to 10 samples per decade. Similarly, ρ_2 varies logarithmically along the vertical axis between $0.1\rho_1$ and $10\rho_1$ in 21 steps. Each template thus represents analyses of $21 \times 21 = 441$ models. In all the analyses, ρ_3 is chosen to be low, equal to $10\,\Omega\mathrm{m}$. Models with values of ρ_3 equal to $100\,\Omega\mathrm{m}$ or $1000\,\Omega\mathrm{m}$ have also been analysed, but for the sake of brevity only models with $\rho_3 = 10\,\Omega\mathrm{m}$ are shown in the following plots.

For all the analyses in Figs 4–9, the top half of the templates represents the maximum models (type-K models), the left quadrant (small thicknesses) being the area where layer suppression and high-resistivity equivalence can be expected, whereas these equivalences disappear on the right side, where the thickness is greater. The bottom half of the templates represents the doubly descending models (type-Q models), and layer suppression can be expected in the left quadrant, where thicknesses are small, and it will gradually disappear on the right side. In general, we must expect the determination of most parameters, especially the parameters of the second layer, to be poorer on the left side of the templates than on the right side.

Choosing the lowest frequency

As far as the choice of the lowest frequency is concerned, we
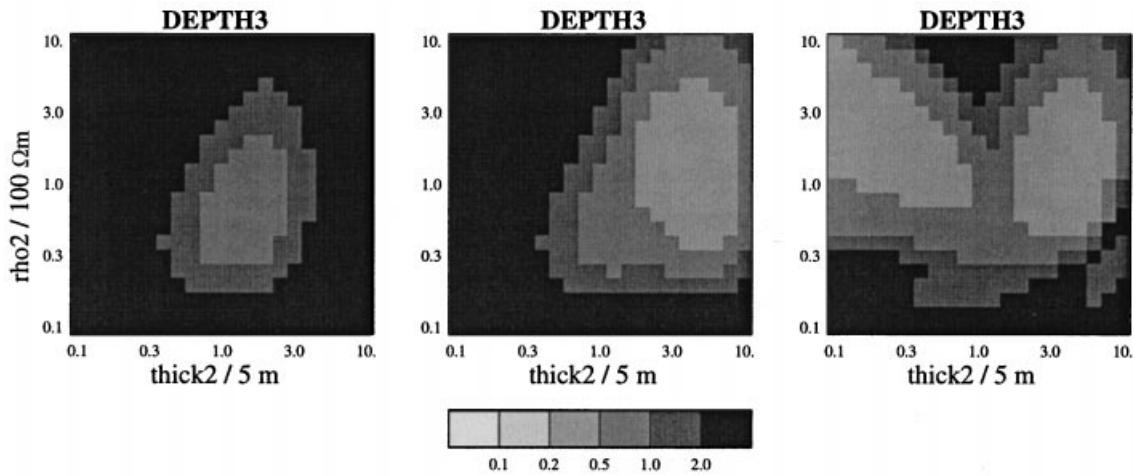
Figure 4 The relative standard deviation of the depth to the third layer of a three-layer model with $\rho_1 = 100\,\Omega m$, $d_1 = 5\,m$ and $\rho_3 = 10\,\Omega m$. The *Tx/Rx* separation is 45 m and a data error of 2% has been assumed. The thickness and the resistivity of the second layer are varied between 0.1 and 10 times the values of the first layer. Left: DC data alone; centre: DC data plus 300 Hz; right: DC data plus 3 kHz.

want to choose it as high as possible to get a signal strength as high as possible and to have as many periods as possible within the time interval of a single measurement to enhance the signal-to-noise ratio. On the other hand, we do not want the frequency to be so high that the resolution improvements in the deeper parts of the model disappear because of the skin effect, giving rise to smaller penetration depths. To determine this limiting frequency a series of analyses of the uncertainty of the depth to a good-conducting third layer was made with one frequency in the interval from 300 Hz to 30 kHz. Selected results are illustrated in Fig. 4.

Figure 4 shows the analysis of the uncertainty of h_3 for galvanic data alone and for galvanic data combined frequencies of 300 Hz and 3 kHz, respectively, for the 45 m *Tx/Rx* separation. With galvanic data alone, it can be seen that h_3 is always undetermined. A marked improvement in the determination of h_3 occurs when just one inductive datum is added to the galvanic data set. For the low frequency, the improvement is seen for models with large d_2. For the higher frequency, an additional region of improvement appears in the upper left-hand quadrant of the template. This improvement increases with increasing
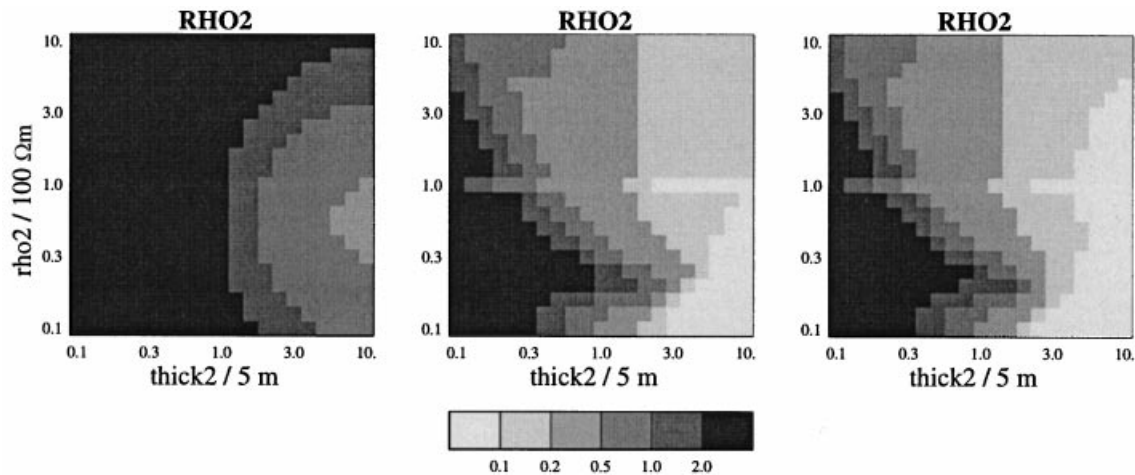
Figure 5 The relative standard deviation of the resistivity of the second layer of a three-layer model with $\rho_1 = 100\,\Omega m$, $d_1 = 5\,m$ and $\rho_3 = 10\,\Omega m$. The *Tx/Rx* separation is 45 m and a data error of 2% has been assumed. The thickness and the resistivity of the second layer are varied between 0.1 and 10 times the values of the first layer. Left: DC data alone; centre: DC data plus 2 and 20 kHz; right: DC data plus 2, 4.309, 9.283 and 20 kHz.
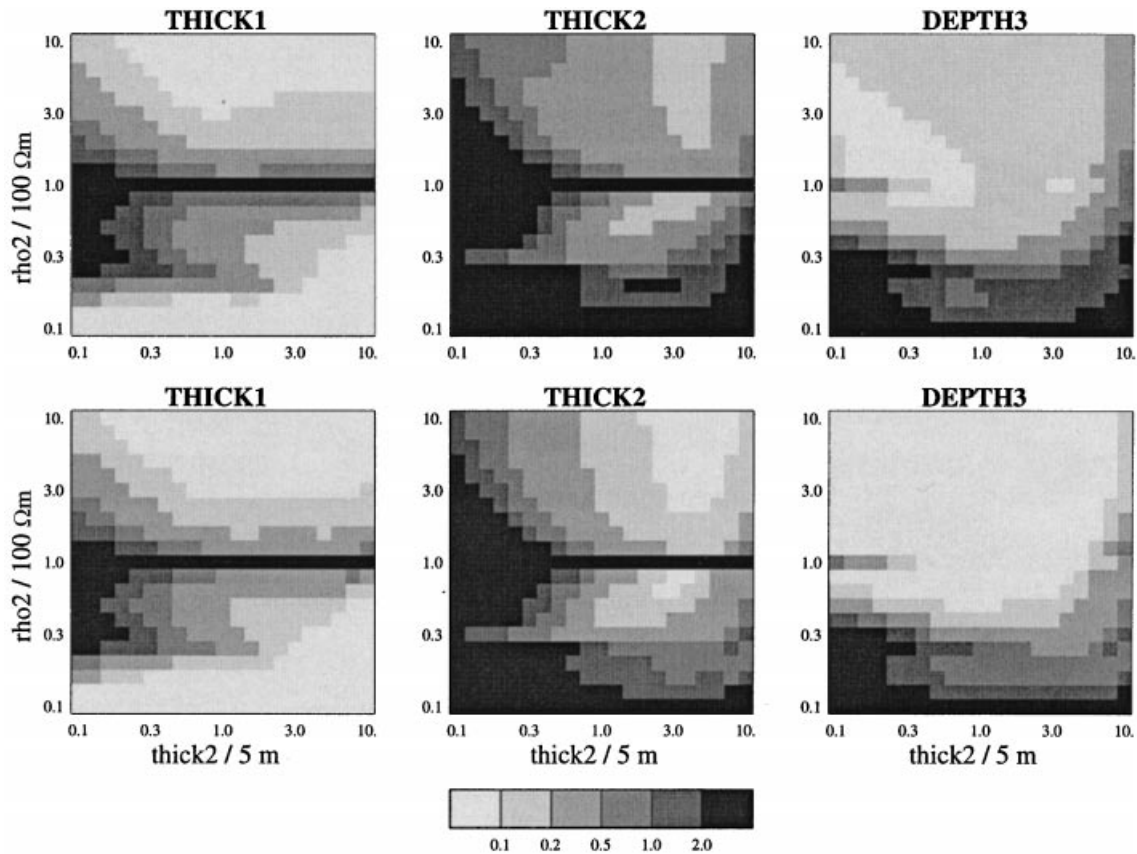
Figure 6 The relative standard deviation of the thickness of the first and second layers and the depth to the third layer of a three-layer model with $\rho_1 = 100\,\Omega\mathrm{m}$, $d_1 = 5\,\mathrm{m}$ and $\rho_3 = 10\,\Omega\mathrm{m}$. Galvanic data plus two frequencies (2 and 20 kHz) have been used and a data error of 2% has been assumed. The thickness and the resistivity of the second layer are varied between 0.1 and 10 times the values of the first layer. The top row is for a *Tx/Rx* separation of 45 m, the bottom row is for a *Tx/Rx* separation of 85 m.

frequency. Up to a frequency of 1–3 kHz, this improvement is gained without appreciable loss for large d_2, since for these low frequencies the penetration depth is determined by the *Tx/Rx* separation and not the frequency. Increasing the frequency beyond a few kHz makes the improvement for large d_2 smaller, due to the onset of the skin effect causing the penetration depth to decrease. Close comparison between the 300 Hz and the 3 kHz plots shows that this effect is just beginning for the frequency 3 kHz. Thus we choose the lowest frequency equal to 2 kHz.

Choosing the number of frequencies

In Fig. 5 the question of the number of frequencies is addressed by investigating the standard deviation of ρ_2 for galvanic data alone, galvanic data plus two frequencies (2 and 20 kHz), and for galvanic data plus four logarithmically spaced frequencies between 2 kHz and 20 kHz (namely 2, 4.309, 9.283 and 20 kHz).

With galvanic data alone, the relative uncertainty of ρ_2 is always greater than 0.5. The figure shows how the addition of two frequencies gives a significant improvement but that the improvement gained by using four frequencies is marginal compared with the case of two frequencies. This is a general feature of the analyses of all model parameters and model parameter combinations for both *Tx/Rx* separations and all three models. By adding the two frequencies, ρ_2 is determined with a relative uncertainty of 10–20% for $d_2 > 1.7d_1$. In the present design study, we therefore choose to have only two frequencies, namely 2 kHz and 20 kHz, since the improvement obtained by adding more frequencies is marginal. In a practical implementation the redundancy obtained by having more than two frequencies will probably be beneficial.

Choosing the *Tx/Rx* distance

Figure 6 shows a comparison between the improvements obtained with the two *Tx/Rx* separations, namely 45 m and
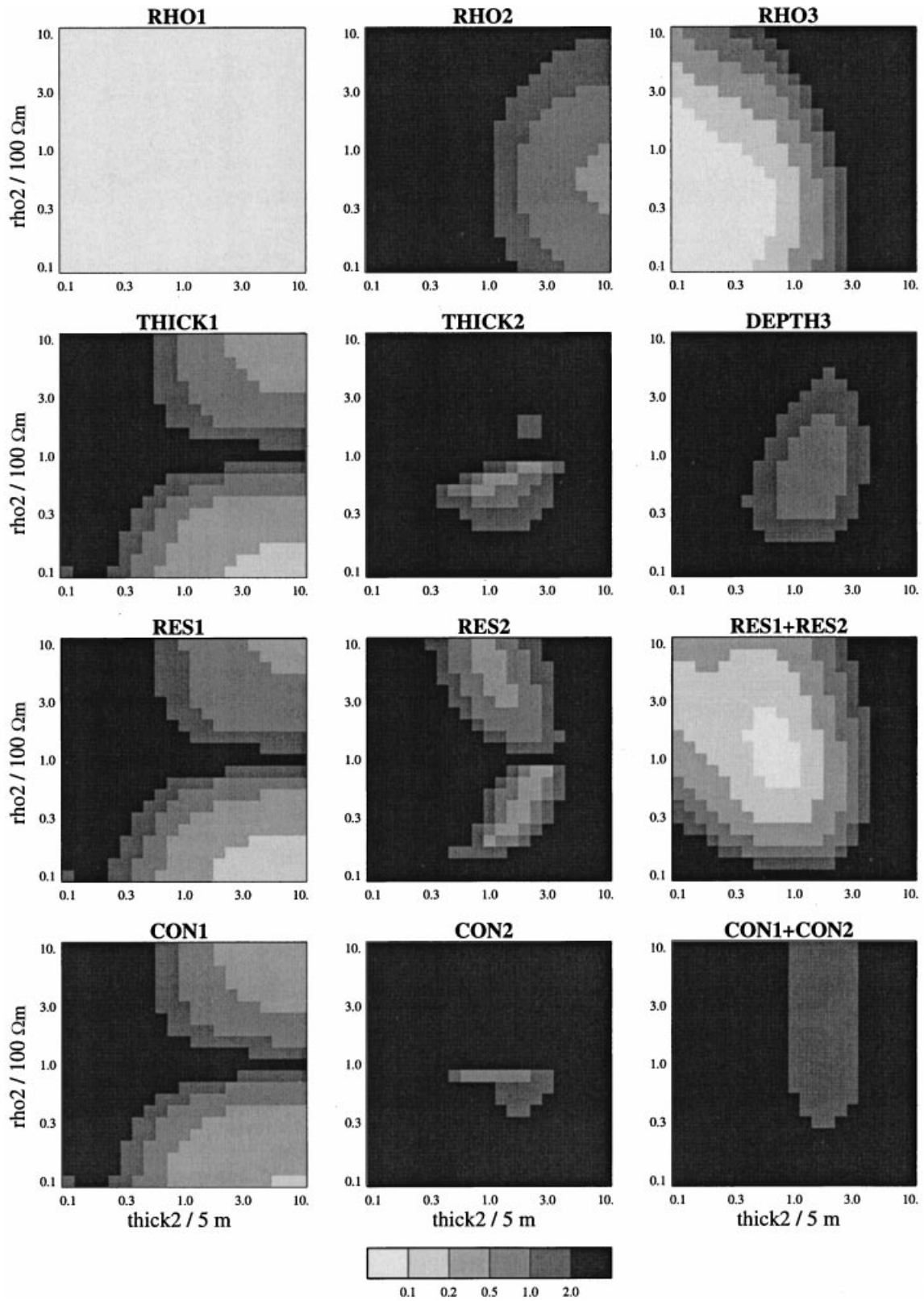
85 m. The analyses show the standard deviations of d_1, d_2 and h_3. Two frequencies, 2 kHz and 20 kHz, were used and $\rho_3 = 10\,\Omega$m. For d_1 there is little difference, but for d_2 and h_3 the longer separation gives a standard deviation which is smaller by a factor of 1.5–2 than that given by the shorter separation. In the templates involving d_1 and d_2, a black horizontal line is seen for $\rho_1 = \rho_2$ indicating that when $\rho_1 \approx \rho_2$, the layer boundary between them is undetermined. For the same reason the bottoms of the templates involving d_2 and h_3, where $\rho_2 \approx \rho_3$, are black, indicating an unresolved layer boundary. These features are also seen in the templates of the following plots.

In general, for the other parameters, an improvement is observed for the longer separation compared with the shorter. Consequently we choose a Tx/Rx separation of 85 m. However, for the model with high bottom resistivity $\rho_3 = 1000\,\Omega$m (not shown here), the difference is marginal.

The final choice of configuration

To sum up, the final configuration of the inductive source will be a horizontal magnetic dipole transmitting the frequencies 2 kHz and 20 kHz and with a Tx/Rx separation of 85 m. The inductive field is measured between the farthest potential electrode 100 m from the source and the electrode 15 m closer to the source. The induction number q for the configuration is given by

$$q = r\sqrt{\omega\mu_0\sigma}, \tag{3}$$

where r denotes the Tx/Rx separation, ω denotes the angular frequency, μ_0 denotes the magnetic permeability of empty space and σ denotes the conductivity. For a half-space with resistivity 100 Ωm and a separation of 85 m, the induction numbers are

$$q_{2\,kHz} = 1.07 \tag{4}$$

and

$$q_{20\,kHz} = 3.38. \tag{5}$$

The lowest frequency is thus slightly above the low-frequency approximation (this was actually the criterion for choosing it), where the depth of investigation is determined by the Tx/Rx separation. The highest frequency is clearly in the inductive region, where the depth of investigation is smaller.

As mentioned above, the potential difference is measured

over a 15 m dipole, 85–100 m from the source. For a frequency of 2 kHz, the amplitude of the potential difference over a 100 Ωm half-space is 2 μV per unit magnetic moment (see Fig. 2). With a magnetic moment of 100 Am^2 which is realizable, the signal strength will be 0.2 mV, sufficient to be measured by a phase-lock amplifier. For the frequency 20 kHz, the signal level will be approximately 10 times higher. Thus the measuring configuration can be realized.

The sensitivity of the configuration will be symmetric about the tail, concentrated in the volumes close to the source and the receiver. Since the current pattern of the horizontal magnetic dipole has many similarities with the horizontal electric dipole perpendicular to it (however with no divergence), the sensitivity will have many similarities to the sensitivity function for the collinear dipole–dipole.

Analyses of the chosen configuration

To conclude the exposition of the analyses, Figs 7 and 8 show analyses of all model parameters and model parameter combinations of the three-layer model set with a low-resistivity bottom layer, $\rho_3 = 10\,\Omega$m. In Fig. 7 galvanic data alone are used and in Fig. 8 the combination of galvanic data and inductive data is used.

For galvanic data alone, most model parameters and combinations are poorly determined or undetermined. Exceptions are the resistivity of the first layer and, for $d_2 < d_1$ and $\rho_2 < \rho_1$, the resistivity of the bottom layer. The summed vertical resistance of the two top layers, RES1 + RES2, also becomes determined for $d_2 \approx d_1$ and $\rho_2 \approx \rho_1$, where it reaches a relative uncertainty of 10%. This is due to the fact that the integrated vertical resistance of the layers over a good conductor is well resolved for galvanic methods. In general, the results of the analyses are not very encouraging, but this must be expected when trying to determine the five parameters of a three-layer model from eight data. Although over-determined, the inversion problem is still ill-conditioned.

A comparison of Figs 7 and 8 demonstrates clearly the improvement obtained when adding a horizontal magnetic dipole source to the PACES equipment.

Although the analyses were carried out under the restriction of using amplitude data alone and not phase, we also investigated the effect of using phase data by including these

Figure 7 The relative standard deviation of all model parameters and model parameter combinations of a three-layer model with $\rho_1 = 100\,\Omega$m, $d_1 = 5$ m and $\rho_3 = 10\,\Omega$m. Only galvanic data have been used and a data error of 2% has been assumed. The thickness and the resistivity of the second layer are varied between 0.1 and 10 times the values of the first layer.
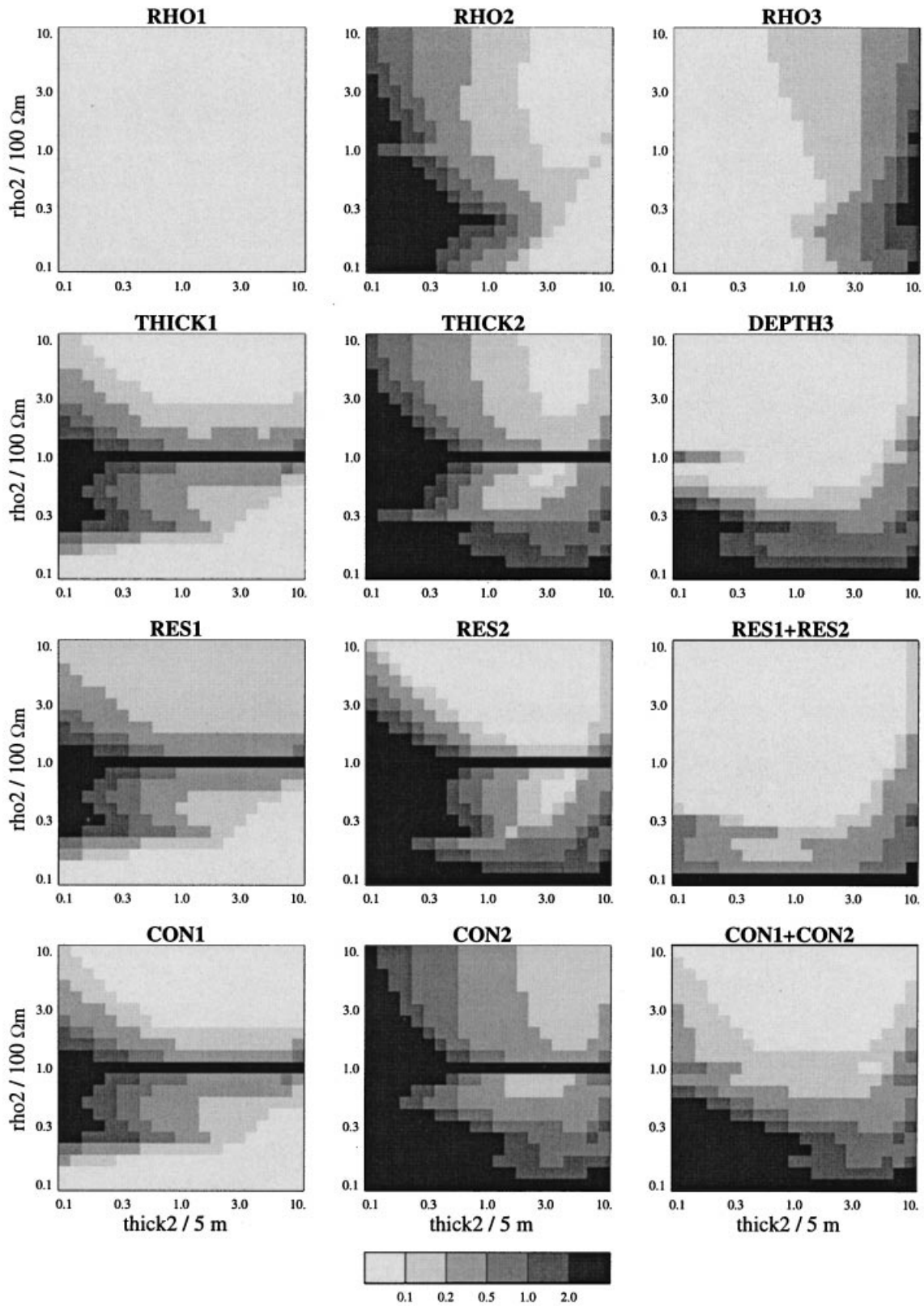
Figure 8 As Fig. 7 but based on galvanic data plus two frequencies (2 kHz and 20 kHz) measured at a *Tx/Rx* separation of 85 m. A data error of 2% has been assumed.
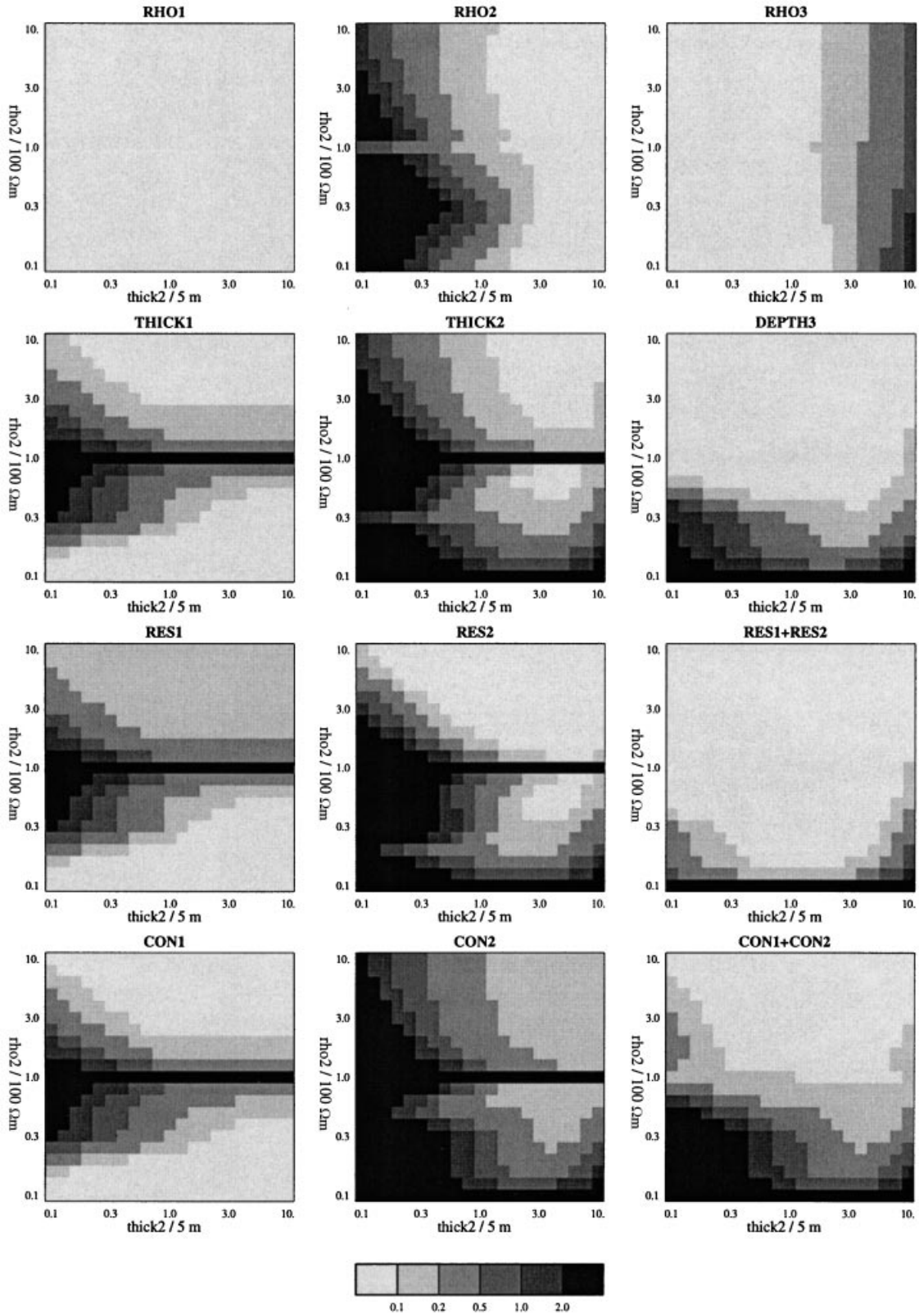
Figure 9 As Fig. 8 but phase data have been included in the analyses. On the galvanic data and the amplitude of the inductive data a data error of 2% has been assumed, while an absolute error of $\pi/200$ has been assumed on the phase data.
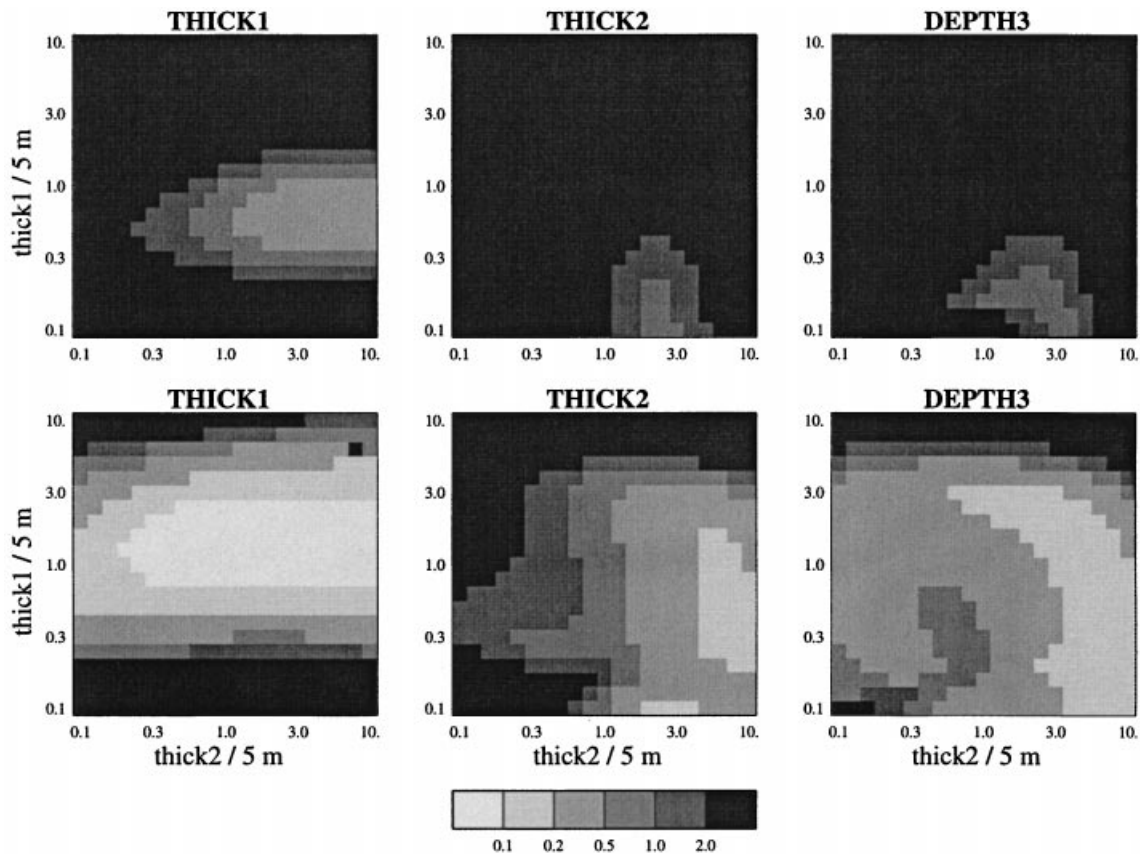
Figure 10 The relative standard deviation of the thickness of the first and second layers and the depth to the third layer of a three-layer model with $\rho_1 = 50\,\Omega\text{m}$, $\rho_2 = 1000\,\Omega\text{m}$ and $\rho_3 = 50\,\Omega\text{m}$. A data error of 2% has been assumed. The thicknesses of the second layer (abscissa) and the first layer (ordinate) are varied between 0.5 and 50 m. The top row is for DC data alone, the bottom row is for DC data plus two frequencies (2 and 20 kHz) with a Tx/Rx separation of 85 m.

in an analysis of the same type as those shown in Figs 7 and 8. The error assumed on the phase was 0.016 rad ($\pi/200$). The result is seen in Fig. 9. It is obvious that phase data are desirable but the improvement is not dramatic compared with the fundamental improvement of including some inductive data. Naturally, if phase data are seriously considered, this single analysis cannot be regarded as comprehensive.

MAPPING OF THIN SAND AND GRAVEL LAYERS

A problem of great importance in connection with hydrogeological investigations of the vulnerability of aquifers, and the mapping of sites where seepage of polluting fluids may be expected to occur, is the presence of thin sand and gravel layers in a confinement clay. Although thin, these layers can, especially if well interconnected, constitute paths of

high hydraulic transmissivity to an underlying aquifer. Such thin layers are normally difficult to resolve due to layer suppression.

A special analysis has been carried out to investigate the improvement in the determination of such layers. We assume $\rho_1 = 50\,\Omega\text{m}$, $\rho_2 = 1000\,\Omega\text{m}$ and $\rho_3 = 50\,\Omega\text{m}$. In the analyses we now vary d_1 and d_2. The Tx/Rx separation is 85 m and we use the frequencies 2 and 20 kHz with amplitude data only. The results are seen in Fig. 10, where the standard deviations of d_1, d_2 and h_3 are shown.

Using exclusively galvanic data, d_1 is the only parameter that will be resolved, but only for $d_1 \approx 3.5\,\text{m}$ and $d_2 > d_1$. The inclusion of inductive data leads to an obvious improvement in the determination of all three parameters when compared with the case of galvanic data alone, but there are still large intervals of parameter values where the standard deviations are high. d_2 is only determined if $d_1 < 15\,\text{m}$ and $d_2 > d_1$.

The choice $\rho_2 = 1000\,\Omega\mathrm{m}$ reflects a sand layer in the vadose zone. Under saturated conditions where conductivity contrasts are smaller, the situation will be even worse.

PROGRAMS FOR JOINT INTERPRETATION

An instrumental design study must be accompanied by considerations concerning the joint interpretation of the new data sets.

Profile data from the PACES system can be interpreted using concatenated 1D interpretations. However, a PACES system with an inductive source can easily produce 10 000 data sets per day, each comprising eight galvanic plus a small number of inductive data; this is a data volume which makes optimization of the 1D interpretation code advisable. Besides being computationally demanding, this approach is also unsatisfactory for a data set which demands, and justifies, at least a 2D interpretation. For dense galvanic profile measurements a linearized 2D deconvolution routine based on the Born approximation and the 2D Fréchet kernel has been developed (Jacobsen 1996; Møller *et al.* 1996, 2001). This deconvolution routine can be extended to include the new additional inductive data, thus offering a very efficient method of approximate joint 2D interpretation of the total data set.

Rigorous 2D interpretation is now carried out for selected parts of special interest of the profiles of galvanic data using the program of Møller (2000). However, new interpretation programs for non-linear 2D joint inversion of the profile data will have to be developed. These must be expected to be computationally quite heavy.

Although anisotropy of the layer resistivities should be taken into account in the joint inversion of galvanic and inductive data (Christensen 2000), for simplicity it has been ignored in the analyses presented here.

CONCLUSION

This study of the improved resolving capabilities obtained by adding a horizontal magnetic dipole source to the PACES equipment shows that considerable improvement can be obtained by the inclusion of just two inductive data. Based on the self-imposed restrictions and the previous analyses, a configuration has been chosen where the amplitude of the horizontal in-line electric field of a horizontal magnetic dipole source with its axis perpendicular to the electrode tail is measured at a *Tx/Rx* distance of 85 m at two frequencies, namely 2 kHz and 20 kHz.

Though one of the assumptions behind the analyses has been that data were amplitude values without phase information, the analysis presented in Fig. 9 shows that phase data will further improve the resolution capabilities. Naturally, the actual improvement will depend on the accuracy with which the phase can be measured.

All analyses made in this study concern 1D models. In the case of multidimensional models, the results can only be regarded as best-case analyses of the vertical resolution capabilities of the measuring system. An analysis of the lateral resolution improvements obtainable with an additional inductive source must be made with 2D and 3D models and is beyond the scope of this paper.

REFERENCES

Christensen N.B. 2000. The determination of electrical anisotropy using surface electromagnetic methods. *Geophysical Prospecting* **48**, 1–20.

Christensen N.B. and Auken E. 1992. SELMA – Simultaneous electromagnetic layered modeling and analysis. In: *Proceedings of Interdisciplinary Inversion Workshop 1 Aarhus 1992, Methodology and Applications within Geophysics, Astronomy, and Geodesy* (ed. B.H. Jacobsen), pp. 49–56. GeoSkrifter, Aarhus University, 41.

Christensen N.B. and Sørensen K.I. 1998. Surface and borehole electric and electromagnetic methods for hydrogeophysical investigations. *European Journal of Environmental and Engineering Geophysics* 3, 75–90.

Edwards L.S. 1977. A modified pseudosection for resistivity and IP. *Geophysics* **42**, 1020–1036.

Fitterman D.V., Meekes J.A.C. and Ritsema I.L. 1988. Equivalence behaviour of three electrical sounding methods as applied to hydrogeological problems. 50th EAEG meeting, The Hague, Netherlands, Expanded Abstracts, p. 37.

Jacobsen B.H. 1996. Rapid 2D inversion by multichannel deconvolution of geophysical profile data. *Proceedings of the Symposium on the Application of Geophysics to Engineering and Environmental Problems, Keystone, Colorado*, pp. 659–668.

Jupp D.L.B. and Vozoff K. 1975. Joint inversion of geophysical data. *Geophysical Journal of the Royal Astronomical Society* **42**, 977–991.

Møller I. 2000. Inversion of 2D geoelectrical data by iterated multichannel deconvolution. In: *Methods and Application of Inversion* (eds P.C. Hansen, B.H. Jacobsen and K. Mosegaard), pp. 217–240. Lecture Notes in Earth Sciences 92, Springer-Verlag, Inc.

Møller I., Christensen N.B. and Jacobsen B.H. 1996. Deconvolution of geophysical multi-offset resistivity profile data. In: *Inverse Methods: Interdisciplinary Elements of Methodology, Computation and Applications* (eds B.H. Jacobsen, K. Mosegaard and P. Sibani), pp. 197–204. Lecture Notes in Earth Sciences, Springer-Verlag, Inc.

Møller I, Jacobsen B.H. and Christensen N.B. 2001. Rapid inversion of 2-D geoelectrical data by multichannel devolution. *Geophysics*, in press.

Møller I. and Sørensen K. 1998. A new approach for fast 2D geoelectrical mapping of near-surface structures. *European Journal of Environmental and Engineering Geophysics* **2**, 247–261.

Oldenburg D.W. 1978. The interpretation of direct current resistivity measurements. *Geophysics* **43**, 610–625.

Raiche A.P., Jupp D.L.B., Rutter H. and Vozoff K. 1985. The joint use of coincident loop transient electromagnetic and Schlumberger sounding to resolve layered structures. *Geophysics* **50**, 1618–1627.

Sandberg S.K. 1993. Examples of resolution improvement in geoelectrical soundings applied to groundwater investigations. *Geophysical Prospecting* **41**, 207–227.

Sørensen K.I. 1995. Pulled array continuous vertical electrical sounding (PACES). *Proceedings of the Symposium on the Application of Geophysics to Engineering and Environmental Problems, Orlando, Florida*, pp. 893–898.

Sørensen K.I. 1996. Pulled array continuous electrical profiling. *First Break* **14**, 85–90.

Ward S.H. and Hohmann G.W. 1987. Electromagnetic theory for geophysical applications. In: *Electromagnetic Methods in Applied Geophysics* (ed. M.N. Nabighian), pp. 131–311. Investigations in Geophysics 3, Society of Exploration Geophysicists.